J. Electrochem. Sci. Eng. **16** (2026) S3153

Open Access : : ISSN 1847-9286
https://pub.iapchem.org/ojs/index.php/JESE

Supplementary material to

Polymer-controlled growth of BiSI/$Bi_{13}S_{18}I_2$ thin films for photoelectrochemical applications

Xeniya Leontyeva, Gulinur Khussurova and Darya Puzikova

D.V. Sokolsky Institute of Fuel, Catalysis and Electrochemistry JSC, Almaty, Kazakhstan

J. Electrochem. Sci. Eng. **16** (2026) 3153; http://doi.org/10.5599/jese.3153

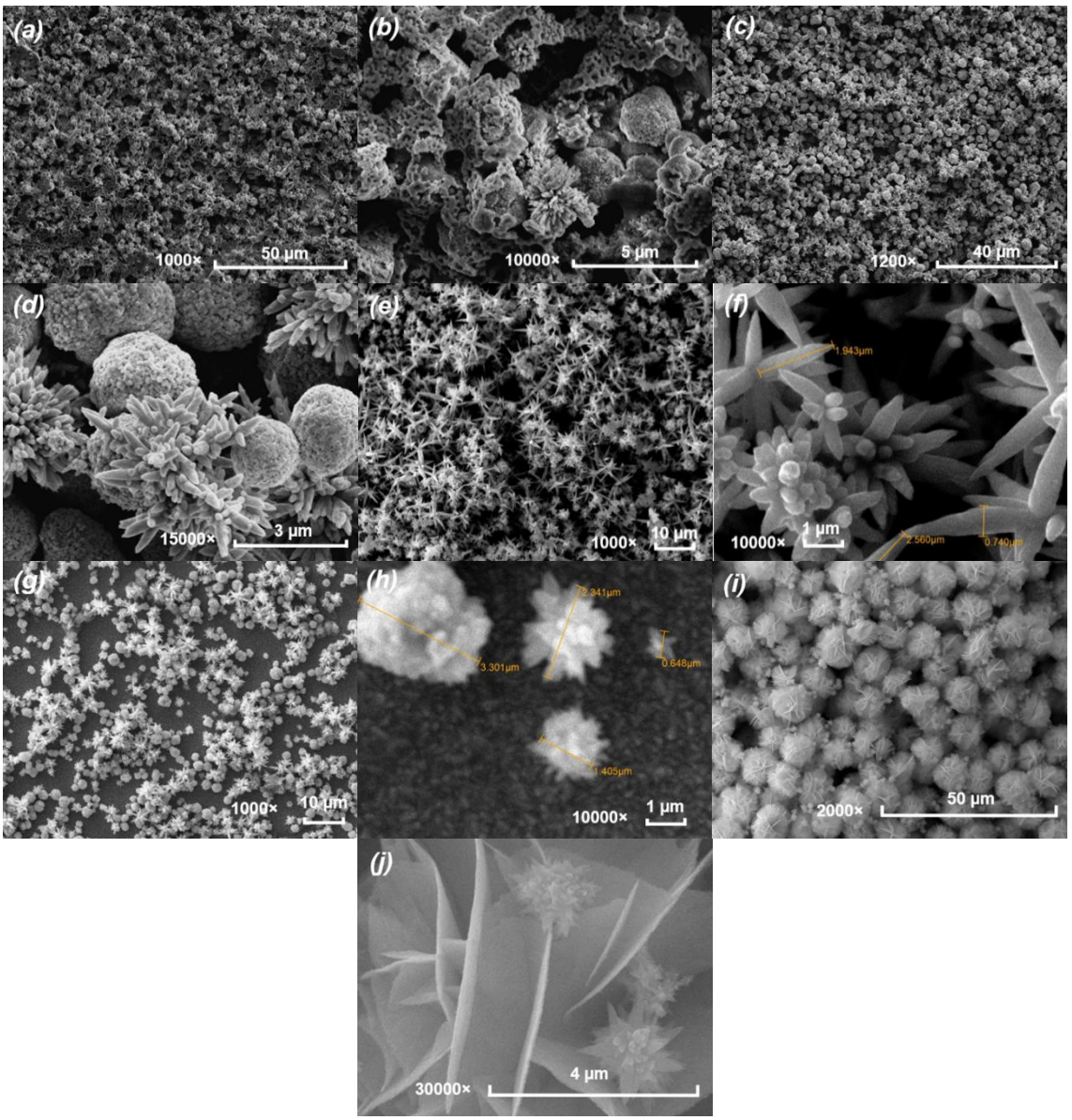

Figure S1. *SEM images of the surface of BiSI/$Bi_{13}S_{18}I_2$ semiconductor thin films synthesized at different PVP concentrations: (a, b) 3.0; (c, d) 2.5; (e, f) 1.6; (g, h) 0.8 and (i, j) 0.0 wt.%*

Table S1 presents the Rietveld refinement results for films prepared at different PVP concentrations. The refinement indicators (R_p, R_{wp}, R_{exp}, χ^2) confirm good agreement between the experimental and calculated patterns. At 2.5 wt.% PVP, the films contain predominantly $Bi_{13}S_{18}I_2$ and BiSI with only minor SnO_2, consistent with their high crystallinity and uniform morphology. Lower PVP contents lead to reduced crystallinity and the appearance of secondary or amorphous phases, while the PVP-free sample is dominated by BiOI (91.6 wt.%) with only small fractions of BiSI and $Bi_{13}S_{18}I_2$. These results underline the stabilizing role of PVP in directing phase formation during CBD.

Table S1. *Quantitative phase analysis and Rietveld refinement parameters for BiSI/$Bi_{13}S_{18}I_2$ thin films deposited via CBD at different PVP contents*

Sample	Unit cell parameter, nm	I_p / %	R_{wp} / %	R_{exp} / %	χ^2	Degree of crystallinity, %	Content, wt. %
3.0 wt.% PVP	a = 1.5612, c = 0.4017	49.8	52.7	34.0	2.4	45.6	SnO_2 - 30.0 $Bi_{13}S_{18}I_2$ - 32.8 BiSI – 20.0 Bi_2S_3 - 17.2
2.5 wt.% PVP	BiSI: a = 0.8460; b = 1.0150, c = 0.4140; $Bi_{13}S_{18}I_2$: a = 1.5612, c = 0.4017	52.6	56.6	101.7	0.3	45.1	SnO_2 - 44.2%; BiSI - 10.8%; $Bi_{13}S_{18}I_2$ - 45.0%
1.6 wt.% PVP	$Bi_{13}S_{18}I_2$: a = 1.5612, c = 0.4017; BiSI: a = 0.8460, b = 1.0150, c = 0.4140; SnO_2: a = 0.4737, c = 0.3201	52.0	57.0	102.1	0.3	40.8	SnO_2 - 65.9 $Bi_{13}S_{18}I_2$ - 24.9; BiSI - 9.2 unidentified - 14.5
0.8 wt.% PVP	BiSI: a = 0.8457, b = 1.0125, c = 0.4117	83.7	72.5	94.6	0.6	38.7	SiO_2 - 47.1 SnO_2 - 29.6 BiSI - 8.8 $Bi_{13}S_{18}I_2$ - 8.0 Bi_2O_2 - 6.4
0 wt.% PVP	BiOI (tetragonal): a = 0.3985, c = 0.9129; BiSI (orthorhombic): a = 0.8460, b = 1.0150, c = 0.4140; $Bi_{13}S_{18}I_2$ (trigonal): a = 1.5612, c = 0.4017	54.6	56.9	87.7	0.421	46.5	BiOI - 91.6 BiSI - 6.5 $Bi_{13}S_{18}I_2$ - 1.9

Table S2 presents a comprehensive comparison of the PEC characteristics obtained in this study with literature data for BiSI-, Bi_2S_3-, BiOI-based photoelectrodes and related heterostructures. Although the IPCE values reported here are lower than some literature data, they were obtained under more conservative and directly comparable conditions. Measurements were performed for single thin films in neutral Na_2SO_4 electrolyte without sacrificial agents, co-catalysts, or complex heterostructures. Therefore, the presented data reflect the intrinsic PEC performance of the BiSI/$Bi_{13}S_{18}I_2$ system and provide a realistic reference for further material optimization.

***Table S2**. Comparison of PEC performance (IPCE/QE/EQE) for BiSI, $Bi_{13}S_{18}I_2$, Bi_2S_3, BiOI and related heterostructures (selected literature data)*

Material/ structure	Deposition synthesis	Electrolyte/conditions	IPCE / EQE, %	Source
BiSI/$Bi_{13}S_{18}I_2$ (heterophase)	Chemical bath deposition (2.5 wt.% PVP)	0.5 M Na_2SO_4; λ = 465 nm, 10 mW cm^{-2}	IPCE = 2.6 ± 0.04	This work (Figures 3-4)
BiSI/$Bi_{13}S_{18}I_2$ (heterophase)	Chemical bath deposition	0.5 M Na_2SO_4 + 0.1 M Na_2SO_3; λ = 465 nm	IPCE = 6.7 ± 0.12	This work
BiSI (low-T conversion from BiOI)	Low-temperature H_2S treatment of BiOI	Acetonitrile solution containing I^- (non-aqueous); λ =700 nm	IPCE = 64	[1]
BiSI	Chemical bath deposition	0.5 M Na_2SO_4; λ = 465 nm	IPCE = 55	[2]
BiSI (micro-rods)	Spray pyrolysis	Device / PV configurations; conditions differ from aqueous PEC	IPCE ≈ 40	[3]
BiSI (needle-like single-crystal film)	Chemical bath deposition	0.05 M Na_2S + 0.05 M KI + 0.5 M Na_2SO_4; halogen lamp; $\lambda \approx$ 400 nm; chopped illumination	EQE = 52	[4]
BiSI (PV devices)	Spin coating	Device testing (λ ~445 to 470 nm, 100 mW cm^{-2})	IPCE ~44	[5]
Bi_2S_3/WO_3 heterojunction	Solvothermal WO_3 + solution coating of Bi_2S_3	0.1 M Na_2SO_4, visible illumination; also 0.2 M NaCl in water-ethanol	IPCE (Na_2SO_4) ~ 14.8 IPCE (NaCl) ~ 9	[6]
Bi_2O_3-BiOI heterojunction	Dipping method	0.2 M Na_2SO_4 for PEC tests; λ = 400 nm; 100 $mWcm^{-2}$	IPCE (Bi_2O_3) = 11; IPCE (BiOI) = 17.5; IPCE (Bi_2O_3-BiOI) = 29	[7]

Table S3 presents the equivalent circuit fitting parameters derived from EIS analysis, allowing direct comparison of interfacial charge-transfer characteristics in different electrolytes. The results indicate that the lowest charge-transfer resistance is observed in Na_2SO_3 electrolyte, whereas the mixed Na_2SO_4/Na_2SO_3 electrolyte exhibits higher R_{ct} despite providing the highest photocurrent, highlighting the complex interplay between interfacial kinetics and hole scavenging processes.

***Table S3.** Equivalent circuit fitting parameters obtained from EIS analysis of BiSI/$Bi_{13}S_{18}I_2$/FTO photoanodes measured under illumination in different electrolytes*

Electrolyte	R_s / Ω	R_{ct} / kΩ	Q (CPE, μF s^{n-1})	n
0.5 M Na_2SO_4	29.4	89.2	16.2	0.89
0.1 M Na_2SO_3	8.17	82.2	1.93	0.91
0.5 M Na_2SO_4 + 0.1 M Na_2SO_3	4.95	279	1.97	0.88

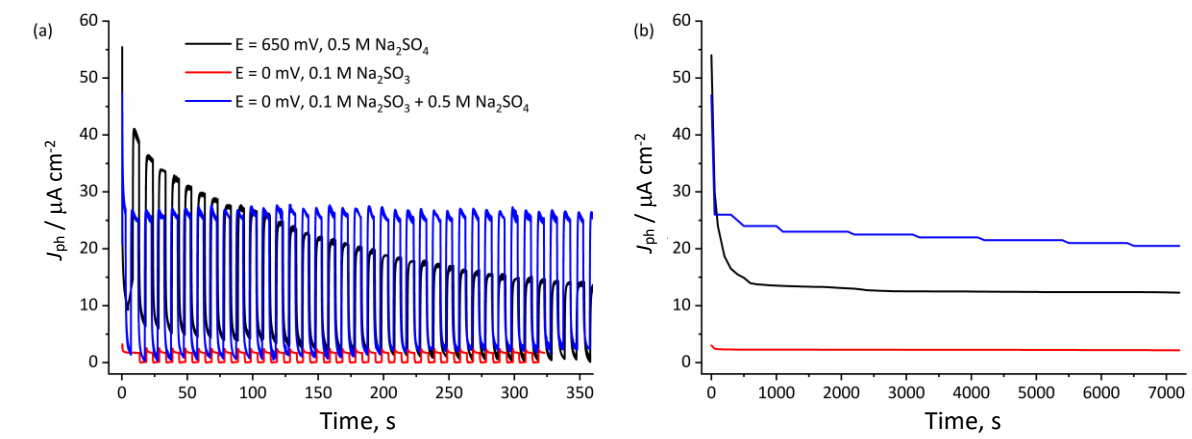

***Figure S2.** Transient and long-term photocurrent stability of BiSI/$Bi_{13}S_{18}I_2$/FTO photoanodes recorded at a fixed potential under chopped blue-light illumination in different electrolytes: (a) short-time transient photocurrent responses (0 to 360 s) and (b) long-term photocurrent stability over 7200 in 0.5 M Na_2SO_4, 0.1 M N Na_2SO_3 and 0.1 M Na_2SO_3 + 0.5 M Na_2SO_4, demonstrating the effect of electrolyte composition on interfacial stability and photocorrosion*

References

[1] H. Kunioku, M. Higashi, R. Abe, Low-temperature synthesis of bismuth chalcohalides: candidate photovoltaic materials with continuously controllable band gap, *Scientific Reports* **6** (2016) 32664. https://dx.doi.org/10.1038/srep32664

[2] M.E. Kazyrevich, D.Y. Ivashenka, E.A. Bondarenko, E.A. Streltsov, A.I. Kulak, Synthesis and photoelectrochemical properties of bismuth thioiodide, *Proceedings of the National Academy of Sciences of Belarus Chemical Series* **54** (2018) 413-418. https://dx.doi.org/10.29235/1561-8331-2018-54-4-413-418

[3] N.T. Hahn, J.L. Self, C.B. Mullins, BiSI micro-rod thin films: Efficient solar absorber electrodes?, *Journal of Physical Chemistry Letters* **3** (2012) 1571-1576. https://dx.doi.org/10.1021/jz300515p

[4] E.A. Bondarenko, A.I. Kulak, A.V. Mazanik, I.A. Svito, E. Streltsov, Photoelectrochemical BiSI-based visible light detector, *Optical Materials* **159** (2025) 116654. https://dx.doi.org/10.1016/j.optmat.2025.116654

[5] V. Sugathan, B. Ghosh, P.C. Harikesh, V. Kotha, P. Vashishtha, T. Salim, A. Yella, N. Mathews, Synthesis of bismuth sulphoiodide thin films from single precursor solution, *Solar Energy* **230** (2021) 714-720. https://dx.doi.org/10.1016/j.solener.2021.10.041

[6] H. He, S. P. Berglund, P. Xiao, W. D. Chemelewski, Y. Zhang, C. B. Mullins, Nanostructured Bi_2S_3/WO_3 heterojunction films exhibiting enhanced photoelectrochemical performance, *Journal Material Chemistry A* **1** (2013) 12826-12834. https://dx.doi.org/10.1039/C3TA13239K

[7] Y. Cong, Y. Ji, Y. Ge, H. Jin, Y. Zhang, Q. Wang, Fabrication of 3D Bi_2O_3-BiOI heterojunction by a simple dipping method: Highly enhanced visible-light photoelectrocatalytic activity, *Chemical Engineering Journal* **307** (2017) 572-582. https://dx.doi.org/10.1016/j.cej.2016.08.114